Dosage compensation and meiotic sex chromosome inactivation are maintained in the absence of selection

Darren J. Parker[1,2], Zoé Dumas[1], Rocío Gómez Lencero[3], Jean-Marc Aury[4], Marjorie Labedan[1], Patrick Tran Van[1], Benjamin Istace[4], Corinne Cruaud[5], Karine Labadie[5], Benjamin Noel[4], Susana Freitas[1], Jelisaveta Djordjevic[1], and Tanja Schwander[1]

1. Department of Ecology and Evolution, University of Lausanne, Lausanne, Switzerland.
2. School of Natural and Environmental Sciences, Bangor University, Bangor, UK.
3. Department of Biology, Universidad Autónoma de Madrid, 28049 Madrid, Spain
4. Génomique Métabolique, Genoscope, Institut François Jacob, CEA, CNRS, Université Evry, Université Paris-Saclay, 91057 Evry, France
5. Genoscope, Institut François Jacob, CEA, CNRS, Université Evry, Université Paris-Saclay, 91057 Evry, France

Abstract

Dosage compensation and meiotic sex chromosome inactivation (MSCI) are key mechanisms regulating gene expression from the X chromosome in male-heterogametic species. While the convergent evolution of these mechanisms is well-documented, their evolutionary fate under relaxed selection remains poorly understood. Here, we test whether dosage compensation and MSCI persist in the absence of selection by investigating three independently derived parthenogenetic species of *Timema* stick insects that occasionally produce rare males. Using chromosome-level genome assemblies, RNA-seq from multiple tissues, and immunocytochemistry, we find that dosage compensation in somatic tissues and meiotic X inactivation are conserved despite the absence of selective pressure in all-female lineages. Surprisingly, expression data and cytological markers indicate that MSCI signatures are even stronger in parthenogenetic males, a pattern driven by prolonged autosomal transcription during meiosis. These results indicate that X-targeting dosage compensation and MSCI mechanisms are either weakly selected against or evolutionarily constrained, while autosomal mis-expressing during meiosis occurs rapidly following the relaxation of selection, shedding light on the stability of X chromosome regulation.

Significance Statement:

Sex chromosomes are regulated by specialized mechanisms that balance gene expression between males and females in somatic tissues (dosage compensation) and silence the X chromosome during male meiosis (meiotic sex chromosome inactivation, MSCI). These processes are thought to decay when they become redundant, yet suitable systems to test this prediction are rare. We studied rare males from parthenogenetic stick insect lineages that have been evolving without sex for up to 1.5 million years. Surprisingly, both dosage

compensation and MSCI remain fully functional, despite relaxed selection. Instead, we find altered autosomal expression during meiosis. Our results reveal that sex chromosome regulation is evolutionarily stable and constrained, persisting even after the loss of its purpose.

Introduction

Sexual reproduction is key to the diversity of life and the main driver of species' lifecycles. In eukaryotic species with distinct male and female sexes, sex determination is frequently governed by sex chromosomes such as X and Y chromosomes in male heterogametic species. Because males carry only a single X chromosome while females carry two, X chromosome expression is regulated by highly specialized mechanisms: dosage compensation (in somatic cells) and meiotic sex chromosome inactivation (MSCI, in germ cells). Dosage compensation is a mechanism that balances the expression of X-linked genes between sexes. It has evolved independently across a wide range of taxa (Disteche, 2012; Mank, 2013; Gu and Walters, 2017) including mammals (Brockdorff and Turner, 2015), reptiles (Marin *et al.*, 2017), fish (Darolti *et al.*, 2019; Metzger *et al.*, 2021), nematodes (Meyer, 2000), and insects (Prince *et al.*, 2010; Conrad and Akhtar, 2012; Vicoso and Bachtrog, 2015; Pal and Vicoso, 2015; Rayner *et al.*, 2021; Chauhan *et al.*, 2021; Parker *et al.*, 2022). However, the X is typically not dosage compensated in gonads, where expression from the sex chromosome(s) is further often suppressed via MSCI (Disteche, 2012; Djordjevic et al., 2024; Mank & Ellegren, 2009; Rayner et al., 2021; Vicoso et al., 2013). Specifically, MSCI involves the inactivation of heteromorphic sex chromosomes during meiosis through the addition of repressive chromatin marks, likely due to the inability of the X and the degraded (or completely lacking) Y to synapse at the onset of meiosis (Burgoyne et al., 2009).

While far from ubiquitous (McKee and Handel, 1993; Mank, 2013), dosage compensation and MSCI are typically maintained across clades for millions of years. Furthermore, a breadth of studies on both mechanisms indicate that they can evolve convergently as new sex chromosomes arise, involving similar or different mechanisms. This is revealed for example by research in dipterans, where X chromosomes have emerged independently from ancestral autosomes, with different dosage compensation mechanisms emerging in parallel (Hamada *et al.*, 2005; Straub *et al.*, 2005; Pease and Hahn, 2012; Davis *et al.*, 2018; Krzywinska *et al.*, 2023; Kalita *et al.*, 2023; Kalita and Keller Valsecchi, 2024; Toups and Vicoso, 2025). Similarly, the independent evolution of MSCI mechanisms in divergent taxa involves both shared and lineage-specific components (e.g. (Namekawa and Lee, 2009; Schoenmakers *et al.*, 2009; Page *et al.*, 2023)).

In contrast to the evidence for the convergent *de novo* evolution of dosage compensation and MSCI, it remains unknown how ancestral dosage compensation and MSCI systems evolve once they become redundant, which would be the case upon the evolution of a novel sex chromosome system. This is in part because suitable model systems with sex chromosome turnovers and accompanying evolution of X-targeting regulatory mechanisms remain understudied. Furthermore, sex chromosome turnover events in species with established dosage compensation and MSCI systems are expected to be rare because the maintenance of active systems could cause extensive misregulation of gene expression on the newly-formed sex chromosomes (Kelley *et al.*, 1995; Lee, 2000; Toups and Vicoso, 2023). A unique opportunity to overcome such constraints is to study the fate and potential decay of dosage compensation and MSCI in all-female parthenogenetic species. Following a transition to parthenogenesis, the X chromosome effectively adopts an autosomal inheritance pattern as it no longer varies in copy numbers since all individuals are female and carry two X copies. As a result, if dosage compensation or MSCI is costly (because of the cost of the machinery or

due to maladaptive expression in females) we would expect selection to reduce a species' ability to perform these mechanisms following a transition to parthenogenesis. Such a reduction is difficult to observe in parthenogenetic species as we need to examine expression in both sexes. This barrier can be overcome in some systems if rare males are produced.

Here we take advantage of such rare males to examine dosage compensation and MSCI in three species of parthenogenetic *Timema* stick insects, using a combination of new chromosome-level genome assemblies, RNA sequencing of eight different tissues, and cell biology. *Timema* have had multiple independent transitions to parthenogenetic reproduction over the last 0.5-1.5 million years (Schwander and Crespi, 2009; Schwander *et al.*, 2011; Bast *et al.*, 2018; Jaron *et al.*, 2022). Previously we have found that sexual *Timema* species show complete dosage compensation in somatic tissues throughout development, and MSCI in the male germline (Parker *et al.*, 2022; Dumas *et al.*, 2024; Djordjevic *et al.*, 2025). This targeted regulation of the X chromosome likely involves general molecular mechanisms shared across insects (Djordjevic *et al.*, 2025) given that the stick insect X chromosome likely evolved prior to the diversification of insects over 450 mya (Toups and Vicoso, 2023). We can examine changes in dosage compensation and MSCI in parthenogenetic *Timema* as they occasionally produce rare males via two different processes. Some males arise from aneuploidy of the X chromosome (Schwander *et al.*, 2013), which since *Timema* have an XX/X0 sex-determination system, results in the production of a male. Others develop as a consequence of very rare instances of sex within parthenogenetic populations (Freitas *et al.*, 2023). Contrary to our prediction we find that the targeted regulation of the X chromosome underlying dosage compensation and MSCI has been conserved in each of the three parthenogenetic lineages, with relaxed selection affecting autosomal rather than X-linked expression in male meiotic cells. These results indicate that selection against X-regulatory mechanisms is weak or that changes to dosage compensation and MSCI mechanisms are highly constrained.

Results and Discussion

Genome assemblies reveal a highly conserved X chromosome contrasted by autosomal fissions and fusions

We generated chromosome-level genome assemblies for two of the three sexual species of *Timema* used in this study, *T. cristinae* and *T. podura*, to complement the available assembly of *T. poppense* (Table S1). In both new assemblies, the number of large scaffolds assembled (hereafter referred to as chromosomes) matched previous karyotype information (Schwander and Crespi, 2009) and coverage of male- vs female-derived short reads were used to identify the X chromosome (Supplemental Info). Annotation using a combination of gene predictions, protein, and RNAseq evidence from each species and its parthenogenetic sister species and inference of 8118 one-to-one orthologs (see Methods) revealed that the X chromosome content has not changed in any of the sexual or asexual species, as expected given the long-term conservation of X chromosome content in stick insects (Simon et al., 2019; Parker et al., 2022). Using comparisons with a stick insect (*Bacillus rossius*) from the Euphasmatodea clade (which split over 120 million years ago from *Timema* (Bank and Bradler, 2022), we further find that even X chromosome synteny is highly conserved, while many rearrangements are apparent on the autosomes (Fig. 1). Specifically, the change in karyotype from 14 to 12 chromosomes during *Timema* evolution (Schwander and Crespi, 2009) involved at least two fissions and three fusions involving *T. podura* chromosomes 2, 3, 5 and 10 (Fig. 1, S1).

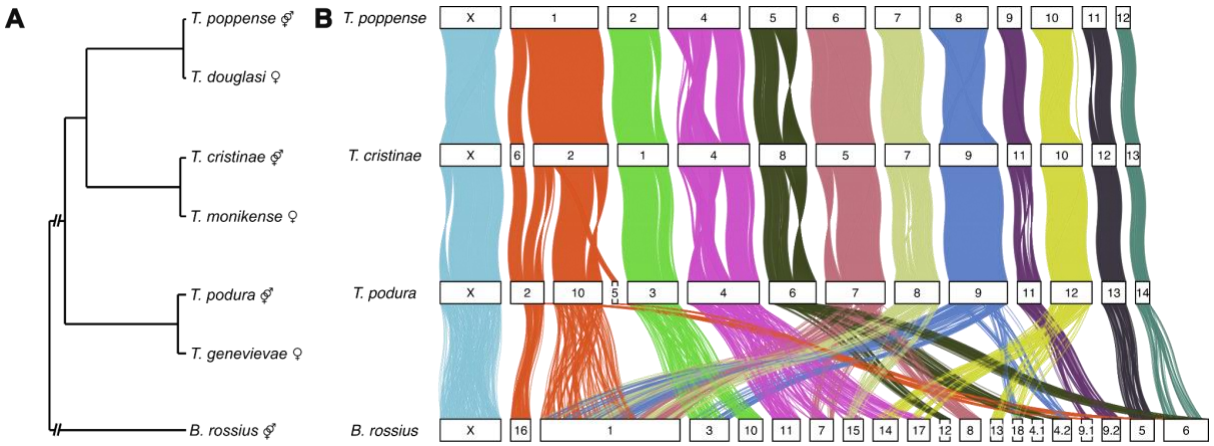

Fig. 1 | Autosomal genomic instability contrasts with X chromosome conservation. A. Simplified phylogeny of the used species, highlighting the independently evolved parthenogenetic *Timema* species and their closest sexual relatives. *Timema* are the sister clade to all other stick insects (including B. *rossius*), and branches reflecting this split have been shortened for display. B. Chord diagram showing synteny between the assemblies of sexual species, based on 4241 one-to-one orthologs across the focal *Timema* genomes and a distantly related stick insect (*Bacillus rossius*). See Fig. S1 for synteny based on 8118 one-to-one orthologs across *Timema* only.

Dosage compensation in somatic tissues is not reduced in parthenogenetic species

Dosage compensation between the sexes in parthenogenetic species was very similar to that observed in sexual species. In all seven non-reproductive tissues (antennae, brain, defence glands, gut, fat body, femur, and tarsi) we observe almost complete dosage compensation in all species (Fig. 2). As expected, we observe some variation in the expression of X-linked genes between the sexes for specific tissues and species (resulting in small but significant differences in expression of autosomal versus X-linked genes). Such variation is typical in studies of dosage compensation (e.g., (Rayner *et al.*, 2021; Hu *et al.*, 2022; Li *et al.*, 2024) and can be interpreted as sex-specific regulation of individual genes rather than a consequence of variable or incomplete dosage compensation. If dosage compensation was reduced in parthenogenetic species, we would expect to see a larger deviation from complete dosage compensation in parthenogenetic species and an accompanying lower male-to-female expression ratio for the X in parthenogenetic species when compared to the sexual sister species for tissues with almost complete dosage compensation. We do not observe this, instead finding only small variations in X-linked expression with no consistent pattern (Fig. 2, Table S2), showing that dosage compensation is maintained across tissues even under relaxed selection for up to 1.5 million years.

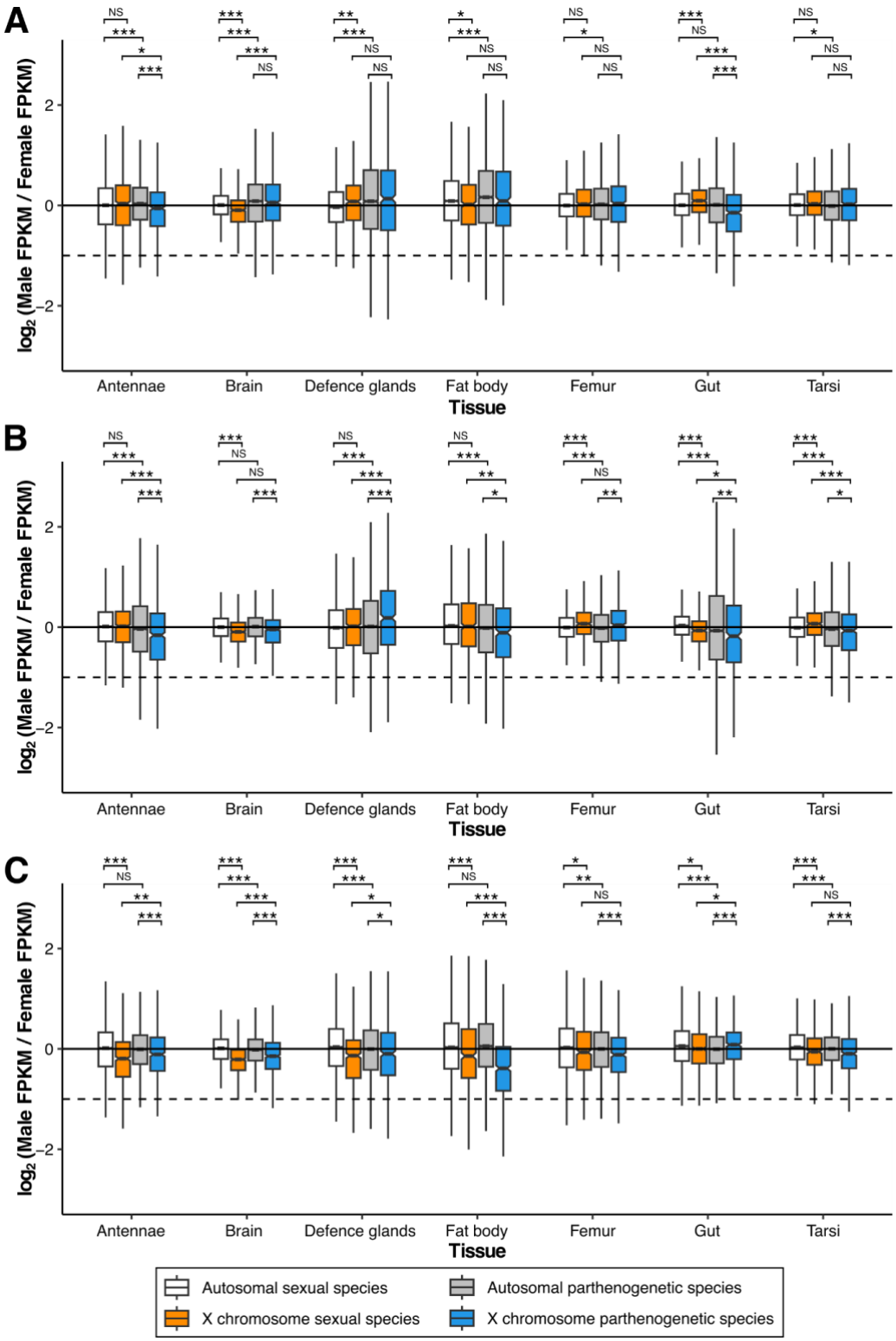

Fig. 2 | Male to female expression ratios for the X and autosomes in non-reproductive tissues reveal the maintenance of dosage compensation under relaxed selection. Dashed lines represent a two- fold reduction in expression in males (as expected if there was no dosage compensation). A. Sexual species = *T. cristinae*, parthenogenetic species = *T. monikense*. B. Sexual species = *T. podura*, parthenogenetic species = *T. genevievae.* C. Sexual species = *T. poppense*, parthenogenetic species = *T. douglasi.* Asterisks indicate the significance (FDR) of Wilcoxon tests (***<0.001, **<0.01, *<0.05, NS > 0.05).

Parthenogenetic species no longer need to perform dosage compensation as all individuals are female and carry the same number of sex chromosomes. Under this scenario, we would expect selection for a reduction in dosage compensation ability for two non-mutually exclusive reasons. Firstly, as the dosage compensation machinery is complex it is likely costly to produce and thus selection should act to remove it when it is no longer needed. One reason we do not observe any consistent changes may be that in insects most of the costs of producing dosage compensation machinery may be in males, as typically dosage compensation is achieved by hyper-transcribing the single X in males (Prince *et al.*, 2010; Conrad and Akhtar, 2012; Mahajan and Bachtrog, 2015; Rose *et al.*, 2016; Richard *et al.*, 2017). That said even if the cost to females was zero we may still expect to see a reduction in dosage composition ability due to the action of drift. We do not see this, which may mean that the genes involved in dosage compensation may be pleiotropic, and alterations therefore deleterious for females. Support for this idea stems from evidence for the maintenance of dosage compensation-like mechanisms targeting the ancestral X in *Drosophila melanogaster* fruit flies (Larsson *et al.*, 2004) even tens of myr after a sex chromosome turnover, which reverted the ancestral X (now referred to as the dot) back to an autosome (Vicoso and Bachtrog, 2015). Similar to our present study in parthenogenetic species, such reversals should result in relaxed selection for dosage compensation on the ancestral X (dot) chromosome. Yet, the dot is still regulated in a chromosome-specific manner, distinct from the other autosomes and the novel X chromosome. Thus, the dot is regulated via the protein POF (Larsson *et al.*, 2004), which might reflect vestiges of the former dosage compensation machinery when the dot was still the X chromosome.

A second reason to expect changes in dosage compensation could be if dosage compensation mechanisms result in maladaptive gene expression in females, i.e., partially unresolved sexual antagonism (Mank *et al.*, 2011). This factor may not have a strong influence in *Timema* as unresolved antagonisms are expected to be transient (Flintham *et al.*, 2025) yet the stick insect X chromosome is very old and highly conserved (Fig. 1) and shares most of its content with the X chromosome in other insect orders that diverged over 450 million years ago (Toups and Vicoso, 2023). Any maladaptive gene expression in females as a result of sexual conflict over dosage compensation would therefore be expected to be very small.

While our results show that dosage compensation is maintained in parthenogenetic species because selection against dosage compensation is weak or because changes to the underlying mechanisms are constrained, we cannot formally exclude that perhaps not enough time has passed since the evolution of parthenogenesis to observe any changes to dosage compensation. While this may be a likely explanation for dosage compensation maintenance across tissues in the young lineage *T. douglasi* and for the lack of apparent changes in dosage compensation in whole-body samples of males of parthenogenetic aphid lineages (Defendini *et al.*, 2025), it is very unlikely for the oldest species used here (*T. genevievae*) with an age estimate of over 1.5 million years (Schwander *et al.*, 2011; Bast *et al.*, 2018). This is likely ample time for even quite gradual changes in dosage compensation to be observed, especially given that *de novo* complete dosage compensation mechanisms can evolve in less than 4 million years (Metzger *et al.*, 2021).

A stronger signature of MSCI in parthenogenetic than sexual species driven by autosomal mis-expression during meiosis

We have shown previously that the X chromosome is consistently inactivated throughout male meiosis in sexual *Timema* species (Dumas *et al.*, 2024; Djordjevic *et al.*, 2025). Accordingly, we observe very low expression of X-linked genes in the testes, much lower than the expectation for a lack of dosage compensation (Fig. 3). We do however still observe some expression of the X in males, as expected given the presence of non-meiotic cells in testes. Surprisingly, we see a consistently lower expression of X-linked genes in males from parthenogenetic than sexual species (Fig. 3). This could indicate a higher proportion of meiotic cells in parthenogenetic than sexual males, or, more likely, that autosomal expression is more persistent across meiosis in parthenogenetic as compared to sexual males. In sexual *Timema* males, there are two bursts of autosomal transcription during meiosis (Dumas *et al.*, 2024): a first at the end of prophase I (specifically, during pachytene and diplotene stages), and a second during meiosis II at the spermatid stage.

To detect potential changes to these temporal patterns of autosomal expression in parthenogenetic males, we performed immunolabeling of testis tissue of *T. monikense* and *T. douglasi* using RNA polymerase II, a conserved transcriptional marker. This labeling revealed that autosomal expression during prophase I is longer in parthenogenetic than sexual males. In the former, the RNA polymerase II signal already appears at the onset of prophase I (i.e., during the zygotene stage; Figs 4, S2) and is maintained until diplotene (Figs 4, S2), while in the latter it only appears at pachytene (Dumas *et al.*, 2024). Since males of parthenogenetic species are not exposed to selection, this extension of the autosomal transcription burst during prophase I is most likely a consequence of drift, i.e., it reflects autosomal mis-expression during meiosis in parthenogenetic males.

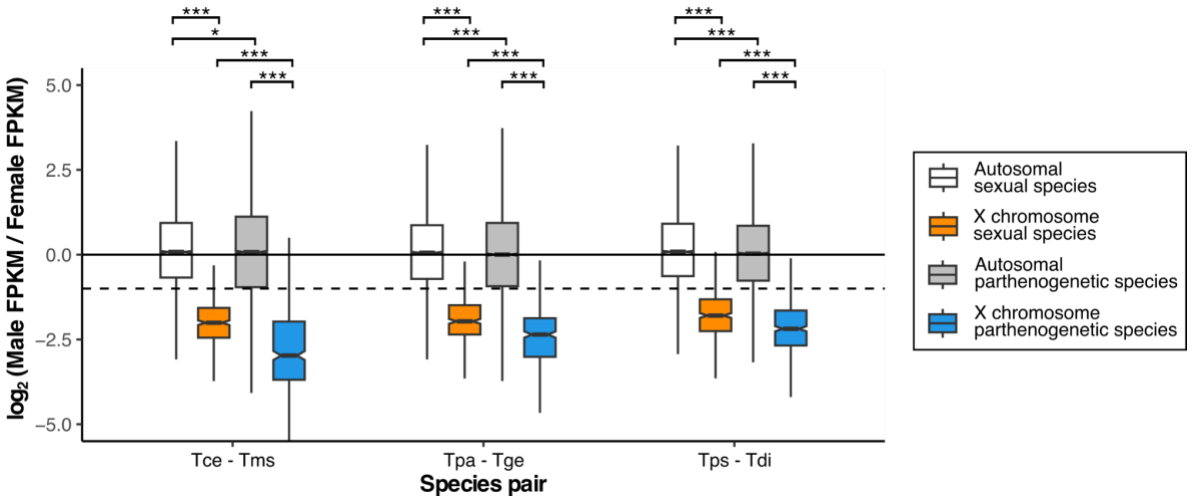

Fig. 3 | A stronger signature of MSCI in parthenogenetic than sexual species. Gene expression in reproductive tissues: Log_2 of male to female expression ratio for the X and autosomes in testes and female gonads. Species codes: Tce = *T. cristinae*, Tms = *T. monikense*, Tpa = *T. podura,* Tge = *T. genevievae,* Tps = *T. poppense* Tdi = *T. douglasi.* Asterisks indicate the significance (FDR) of Wilcoxon tests (***<0.001, **<0.01, *<0.05, NS > 0.05).

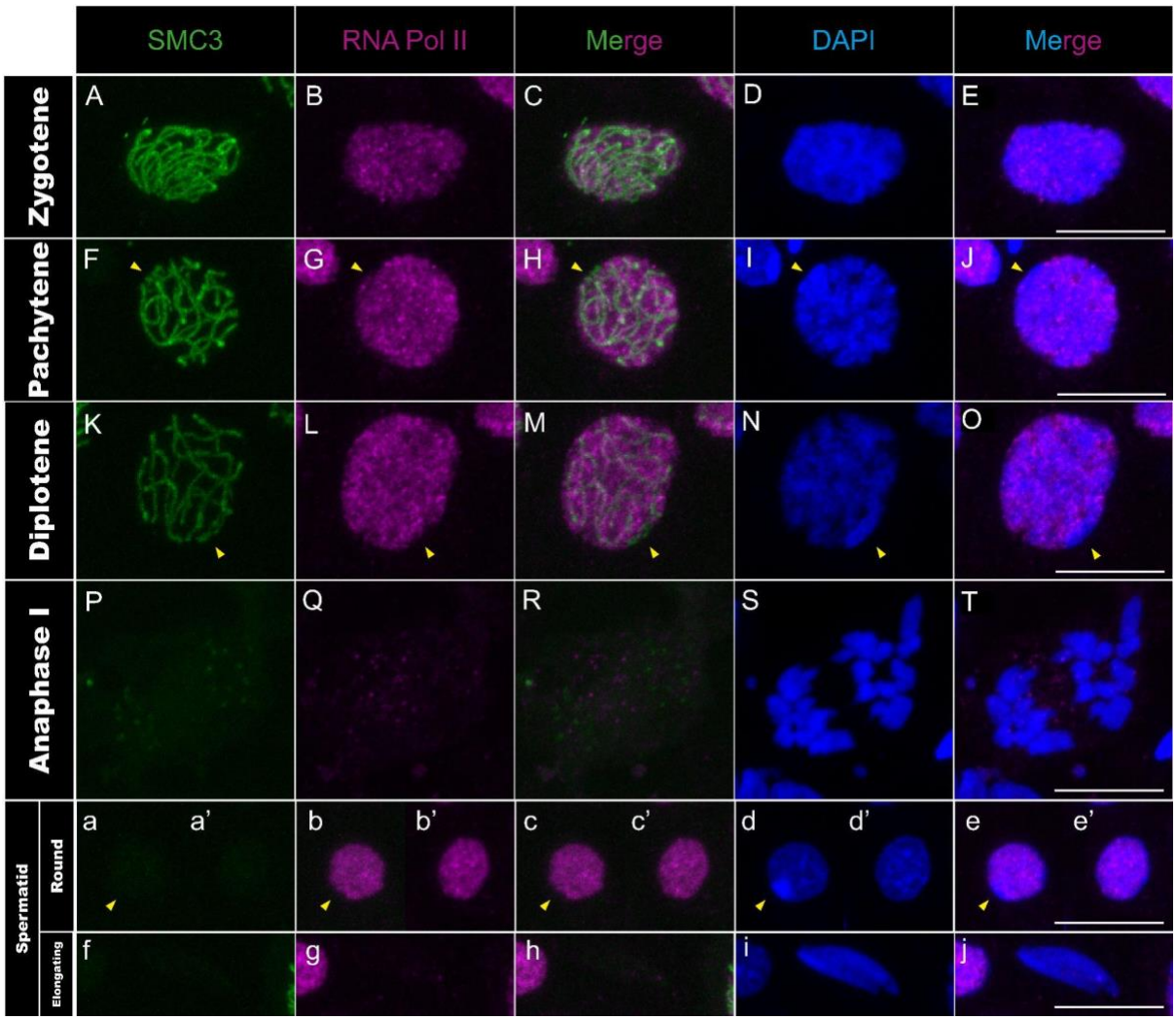

Fig. 4 | Misregulation of autosomal gene expression in meiotic cells of parthenogenetic males. RNApol-II distribution in *T. monikense* meiocytes and spermatids. Projections of stack images acquired across *T. monikense* squashed meiocytes (A–T) and spermatids (a–e'), at the stages indicated, stained with DAPI (blue) and double immunolabeled for SMC3 (green) and RNApol-II (magenta). RNApol-II labelling is intense from zygotene to diplotene, and in the round spermatid stage. During all spermatogenesis stages, the X chromosome is extremely reduced in RNApol-II labelling. The position of the X chromosome is indicated with arrowheads. Scale bar: 10 µm. Corresponding image analyses for males of *T. douglasi* are available in Fig. S2)

Conclusion

Our results demonstrate that both dosage compensation and meiotic sex chromosome inactivation (MSCI) are robustly maintained in parthenogenetic stick insects, despite the long-term absence of selective pressures typically associated with male phenotypes. This maintenance suggests that the molecular mechanisms underlying dosage compensation and MSCI are either functionally constrained, potentially due to pleiotropic effects in females, or maintained through weak purifying selection. Notably, the enhanced signature of MSCI in parthenogenetic males appears to be driven by extended autosomal transcription during meiosis, revealing an unexpected consequence of relaxed selection on gene expression. Together, these findings highlight the stability and evolutionary inertia of complex regulatory processes, even in the face of dramatic shifts in reproductive mode.

Methods

Reference genome assemblies

Reference genome assemblies were produced for *T. cristinae* (Bioproject PRJNA1268975/ Accession JBOIUC000000000) and *T. podura* (Bioproject PRJNA1268975/ Accession JBOIUD000000000) from wild collected females (GPS coordinates 34°30'53.2"N, 119°46'45.3"W and 33°47'47.0"N, 116°46'34.6"W). Contigs for the *T. cristinae* assembly were based on PacBio sequencing (43x) and on a combination of Nanopore and Illumina sequencing for *T. podura* (sequenced at 85x respectively 62x coverage). Scaffolding was done using a Hi-C library (sequenced at approximately 69 x and 53 x coverage for *T. cristinae* and *T. podura* respectively) to produce the final reference assembly.

DNA extraction and library preparation

To extract high molecular weight (HMW) DNA, we flash-froze a single female (without gut) in liquid nitrogen and ground it using a Cryomill (Retsch). We then extracted HMW DNA using a G/20 Genomic Tips kit (Qiagen) following the manufacturer's protocols and checked DNA integrity on a pulse field agarose gel.

For *T. cristinae*, a PacBio library was prepared using the Template Prep Kit 1.0 following manufacturer's instructions and sequenced on a single cell of the PacBio SMRT™ system. For *T. podura*, four ONT libraries were prepared following Oxford Nanopore instructions. A first library was prepared using the SQK-LSK108 ligation sequencing kit and was loaded on a MinION R9.4 Flow Cells, and then three libraries were prepared using the SQK-LSK109 ligation sequencing kit and were loaded on three PromethION R9.4.1 Flow Cells. A PCR free Illumina library (based on the same HMW extraction) was prepared using the Kapa Hyper Prep Kit (Roche, Basel, Switzerland), following manufacturer instructions. The library was quantified by qPCR using the KAPA Library Quantification Kit for Illumina Libraries (Roche), and the library profile was assessed using a High Sensitivity DNA kit on an Agilent Bioanalyzer (Agilent Technologies, Santa Clara, CA, USA). The library was then sequenced on an Illumina HiSeq 4000 instrument (Illumina, San Diego, CA, USA), using 150 base-length read chemistry in a paired-end mode.

A Hi-C library was prepared for each species using the Proximo Hi-C Kit. We generated ground tissue for cross-linking using Cryomill (Retsch) and following manufacturer instructions, using a different female than the one used for Nanopore and HiSeq sequencing, from the same natural population. Library construction and sequencing (250 million read pairs) was outsourced to Phase Genomics (Seattle).

Assembly pipelines

We used different strategies for genome assembly for the two species. For *T. cristinae* raw PacBio reads were assembled into contigs using Canu (Koren *et al.*, 2017) with the parameter correctedErrorRate=0.105. For *T. podura* raw Oxford Nanopore reads were filtered using Filtlong v0.2.0 (https://github.com/rrwick/Filtlong) with the parameters --min_length 1000 --keep_percent 90 --target_bases 69050000000. The filtered Nanopore reads were then assembled into contigs using Flye v2.8.1 (Kolmogorov *et al.*, 2019) with --genome-size 1.381g. All Nanopore reads were mapped against the contigs using minimap2 v2.19 (Li, 2018) with the parameters -c -x map-ont and a first step of polishing was performed using Racon v1.4.3 (Vaser *et al.*, 2017). Three additional rounds of polishing were conducted: Illumina short reads were aligned to the contigs using BWA mem v0.7.17 (Li, 2013) and polishing was performed using Pilon v1.23 (Walker *et al.*, 2014).

Both assemblies were then decontaminated using BlobTools v1.0 (Laetsch and Blaxter, 2017) under the taxrule “bestsumorder”. Hit files were generated after a blastn v2.10.1+ against the NBCI nt database, searching for hits with an e-value below 1e-25 (parameters: -max_target_seqs 10 -max_hsps 1 -evalue 1e-25). Contigs without hits to metazoans were removed from the assemblies. Haplotypic duplications were then filtered out as follows. Filtered reads were then mapped against the decontaminated genomes using minimap2 and haplotigs were detected with Purge Haplotigs v1.1.1 (Roach *et al.*, 2018) using the parameters -l 3 -m 27 -h 190 -j 101 --editor-coarse-resolution 250000 for *T. cristinae* and -l 3 -m 45 -h 195 -j 101 --editor-coarse-resolution 50000 for *T. podura*.

Hi-C reads from each species were then mapped against their respective haploid genome using Juicer v1.6 (Durand *et al.*, 2016) with the restriction site Sau3AI. Finally, chromosome-level scaffolding was performed using 3D-DNA v180922 (Dudchenko *et al.*, 2017) with species-specific parameters, as recommended by the authors. The resulting Hi-C contact matrices were visualized with Juicebox, and minor polishing was conducted in accordance with these recommendations. The completeness of both genome assemblies was assessed with BUSCO v5.1.2 (Seppey *et al.*, 2019) against the *insecta_odb10* dataset using the --long and --augustus parameters.

Annotation

We annotated the *T. cristinae* and *T. podura* genomes in a similar way as we previously annotated the *T. poppense* genome (Djordjevic *et al.*, 2025), using a combination of *ab initio* gene prediction, protein homology, and RNA-seq using the Braker2 pipeline (v. 2.1.6) (Brůna *et al.*, 2021). Firstly, each genome assembly was soft-masked using RepeatModeler (v. 2.0.2,

365 options: -LTRStruct, -engine ncbi) (Flynn *et al.*, 2020) and RepeatMasker (v. 4.1.2, options: -
366 engine ncbi, -xsmall) (Smith *et al.*, 2013). For protein evidence, we used the arthropod protein
367 sequences from OrthoDB (v.10.1) (Kriventseva *et al.*, 2019) and the predicted protein
368 sequences for *Timema* from our previous genome assemblies. For RNAseq evidence, we
369 used the RNAseq libraries generated here for *T. cristinae* and *T. monikense* along with publicly
370 available data (163 libraries generated here, 43 public (Bioproject accessions: PRJNA380865,
371 PRJNA679785, PRJNA1295360, PRJNA504764 (Bast *et al.*, 2018; Parker *et al.*, 2019; Jaron
372 *et al.*, 2022))) to annotate the *T. cristinae* genome and for *T. podura* and *T. genevievae* (119
373 libraries generated here, 29 public (Bioproject accessions: PRJNA380865, PRJNA679785,
374 PRJNA1295360 (Bast *et al.*, 2018; Jaron *et al.*, 2022))) to annotate the *T. podura* genome.
375 This is a total of 354 RNAseq libraries (330 paired-end, 24 single-end) covering over 19
376 different life stages, tissue, and sex combinations for each species (see Table S3). Reads
377 were quality trimmed with Trimmomatic (v. 0.39, options: ILLUMINACLIP:3:25:6 LEADING:9
378 TRAILING:9 SLIDINGWINDOW:4:15 MINLEN:80) (Bolger *et al.*, 2014) before mapping to the
379 genome assembly with STAR (v. 2.7.8a, options: --twopassMode Basic) (Dobin *et al.*, 2013).
380 Braker2 was run using protein evidence and RNAseq separately with the gene predictors
381 Augustus (v. 3.4.0) (Stanke *et al.*, 2006) and Genemark (v. 4.72) (Brůna *et al.*, 2020).
382 Following the RNAseq run, UTR predictions were added to the RNAseq gene predictions using
383 GUSHR (v. 1.0) in Braker2 (--addUTR=on). The separate gene predictions were then merged
384 using TSEBRA (v1.0.3) using the pref_braker1.cfg configuration file, which weights RNAseq
385 evidence more strongly than the default option. We then ran BUSCO (v. 5.3.2, insecta_odb10)
386 on the gene regions annotated by Braker2 and on the whole genome assembly. Any genes
387 found by BUSCO but missed by Braker were then added to the annotation (69 genes for *T.*
388 *cristinae* and 19 genes for *T. podura*). ncRNA genes were predicted using Infernal (v. 1.1.2,
389 minimum e-value 1e-10) (Nawrocki and Eddy, 2013). GO-terms for protein-coding gene
390 predictions were obtained using blastP within OmicsBox (v3.1.2, default parameters) to blast
391 the nr *Drosophila melanogaster* database (taxonomy filter: 7227). 1-to-1 orthologs between
392 were obtained for protein-coding genes using OrthoFinder (version 2.5.5) (Emms and Kelly,
393 2019) with default options.

394 ***Identification of the X chromosome***

395

396 We used a coverage approach to identify X-linked scaffolds in our new genome assemblies.
397 To do this we mapped publicly available Illumina genome reads from males and females (4
398 males and 5 females for *T. cristinae* and 4 males and 2 females for *T. podura* (PRJNA670663,
399 PRJNA725673 (Jaron *et al.*, 2022; Parker *et al.*, 2022)) to the respective genome assemblies
400 and their publicly available mtDNA genomes using BWA-MEM (v. 0.7.15). Multi- mapping and
401 poor quality alignments were filtered (removing reads with XA:Z or SA:Z tags or a mapq <30).
402 PCR duplicates were removed with Picard (v. 2.9.0) (http://broadinstitute.github.io/picard/).
403 Coverage was then estimated for 100000 bp sliding windows using BEDTools (v. 2.26.0)
404 (Quinlan and Hall, 2010). To compare coverage between males and females, coverage was
405 first summed for all male and all female libraries per window. Male and female coverage was
406 then normalized by modal coverage to adjust for differences in overall coverage. X- linked
407 windows were then identified using the $\log_2$ ratio of male to female coverage. Autosomal
408 windows should have equal coverage in males and females ($\log_2$ ratio of male to female
409 coverage ≈ 0) and X-linked windows should have half the coverage in males as in females

410 (log2 ratio of male to female coverage ≈ −1). This approach identified one large scaffold in
411 each assembly as the X chromosome (Fig. S3-5).
412
413 We then repeated these analyses using genome reads from each of the parthenogenetic
414 species. Female reads were publicly available (5 for *T. monikense*, 6 for *T. genevievae*, and
415 5 for *T. douglasi*, PRJNA670663 (Jaron *et al.*, 2022)) as were the two male samples for *T.*
416 *douglasi* (PRJNA808673, (Larose *et al.*, 2022)). For *T. monikense* and *T. genevievae* we also
417 generated new Illumina libraries for males (2 for *T. genevievae* and 4 for *T. monikense*) and
418 an additional female library for *T. genevievae* (Accession number: PRJNA1293928) as
419 described previously (Jaron *et al.*, 2022) using the carcasses after tissue dissection described
420 below. Reads were then mapped to the genome of each sexual sister species as described
421 above (the sexual species genome for *T. douglasi* is our previously published genome *T.*
422 *poppense,* Accession number: PRJNA1126215 (Djordjevic *et al.*, 2025)). Each of the newly
423 generated samples were checked for normal coverage distributions before calculating
424 coverage ratios.
425

426 ***RNA extraction and sequencing***

427
428 We generated a total of 282 RNA-seq libraries for eight female tissues (antennae, brain,
429 defence glands, fat body, femur, tarsi, and gonads) and nine male tissues (the same as the
430 female plus the male accessory glands) for *T. cristinae*, *T. podura*, *T. monikense*, and *T.*
431 *genevievae* following our previously developed methodology (Djordjevic *et al.*, 2025) (see
432 Table S3 for details). Individuals were collected as nymphs in the field and reared to adulthood
433 in the laboratory. Prior to dissection all individuals were isolated in Petri dishes and fed on an
434 artificial diet (a mix of flour, sugar, and water) for two days, allowing their gut contents to be
435 cleared of plant material. Insects were then anesthetized with CO_2, dissected, and tissues
436 individually flash-frozen in liquid nitrogen before being stored at -80°C.
437
438 TRIzol solution (1 mL) and a small amount of ceramic beads (Sigmund Lindner) were added
439 to each tissue. Samples were homogenized using a tissue homogenizer (Precellys Evolution;
440 Bertin Technologies). Chloroform (200 µL) was added to each sample and samples were then
441 vortexed for 15 seconds and centrifuged for 25 minutes at 12,000 rpm at 4°C. The upper
442 phase containing the RNA was then transferred to a new 1.5 mL tube with the addition of
443 isopropanol (650 µL). The samples were vortexed and placed at -20°C overnight. Samples
444 were then centrifuged for 30 minutes at 12,000 rpm at 4°C. The liquid supernatants were
445 removed, and the RNA pellet underwent two washes using 80% and 70% ethanol. Each wash
446 was followed by a 5-minute centrifugation step at 12,000 rpm. Finally, the RNA pellet was
447 resuspended in nuclease-free water and quantified using a fluorescent RNA-binding dye
448 (QuantiFluor RNA System) and nanodrop (DS-11 FX).
449
450 Library preparation using NEBNext (New England BioLabs) and sequencing on an Illumina
451 NovaSeq 6000 platform with 100 bp paired-end sequencing (36.2 million read pairs per
452 sample on average) was outsourced to a sequencing facility (Fasteris, Geneva).
453

454 ***Gene expression analyses***

455

456 We mapped RNAseq reads from *T. cristinae*, *T. podura*, *T. monikense*, and *T. genevievae*
457 generated here and reads for *T. poppense* and *T. douglasi* we generated previously
458 (Djordjevic *et al.*, 2025) to their respective genomes as described above. This gave 4
459 replicates for each of the 16 sex and tissue combinations for each of the six species, except
460 for the male samples of parthenogenetic species (*T. monikense, T. genevievae,* and *T.*
461 *douglasi*) where we had fewer replicates due to the difficulty of obtaining these specimens (n
462 = 2-4 see Table S4 for details). Read counts were obtained using HTSeq v.0.9.1 (Anders *et*
463 *al.*, 2015), with the following options (htseq-count --order = name --type = exon --idattr =
464 gene_id --stranded = reverse). Expression analyses were performed using the Bioconductor
465 package EdgeR (v 3.42.4) (Robinson *et al.*, 2010), and done separately for each species and
466 tissue. Normalization factors for each library were computed using the TMM method and were
467 used to calculate normalized expression levels (FPKM, Fragments Per Kilobase of transcript
468 per Million mapped reads). mtDNA, rRNA, tRNA and genes with low expression (less than 2
469 FPKM in 2 or more libraries per sex) were excluded. To examine dosage compensation, we
470 used the $\log_2$ ratio of mean male expression level to female expression level and used
471 Wilcoxon tests (adjusted for multiple testing using Benjamini and Hochberg's (1995) algorithm)
472 to determine if differences in expression between the autosomes and the X chromosome were
473 significant.

474

475 ***Immunolabeling of parthenogenetic male meiotic cells***

476

477 In order to determine the dynamics of autosomal gene expression during meiosis in
478 parthenogenetic males, we followed the same protocol previously used to characterize
479 autosomal gene expression during meiosis in sexual males (Dumas *et al.*, 2024). In brief, we
480 performed double immunolabeling of SMC3_488 (#AB201542, AbCam) as a marker of
481 cohesin axes (this allows for the assessment of synapsis progression, and hence, cell cycle
482 stage) and RNA polymerase II phosphorylated at serine 2 (p-RNApol-II (ab193468, AbCam);
483 an indicator of transcription). Gonads from adult *T. monikense* and *T. douglasi* males were
484 dissected in 1X PBS, then fixed in paraformaldehyde (2%) and Triton X-100 (0.1%) solution
485 for 15 minutes. Gonads were then squashed on slides coated with poly-L-lysine, and flash
486 frozen in liquid nitrogen. Slides were incubated in PBS 1x for 20 minutes at room temperature,
487 then blocked with a BSA 3% solution (prepared by dissolving 3g of BSA in 100mL of PBS 1X)
488 for 20 minutes. Slides were then incubated overnight at 4°C in a humid chamber with the
489 primary (p-RNA-Pol II), diluted in BSA 3% (1:100), and washed 3x for 5 minutes in PBS 1X.
490 The secondary antibody, anti-rabbit Alexa 594 (711-585-152, Jackson), diluted in BSA 3%
491 (1:100), was applied, and samples were incubated for 45 minutes at room temperature.
492 Further washes were conducted as described above, followed by an extended 10-minute wash
493 in PBS 1X, and by blocking using a 5% Normal Rabbit Serum (NRS) solution (X090210-8,
494 Agilent Technology) for 30 minutes at room temperature. Another 5-minute wash in PBS 1x
495 was performed to remove excess blocking solution. Samples were then incubated with the
496 labelled antibody SMC3_488 (#AB201542, AbCam) at a 1:100 dilution for 1 hour at room
497 temperature, followed by a final series of washes and staining with DAPI (D9542, Sigma-
498 Aldrich) for 3 minutes at room temperature. Finally, after a 5-minute wash in 1x PBS, two drops
499 of Vectashield were added to the slide, which was then covered with a coverslip, and sealed

with nail varnish for imaging. Image acquisition was performed at the Cellular Imaging Facility (CIF, University of Lausanne) using a Zeiss LSM 880 Airyscan.

Data

Genome assemblies have been deposited at DDBJ/ENA/GenBank under the accessions JBOIUC000000000 (*T. cristinae*) and JBOIUD000000000 (*T. podura*). The Illumina and PromethION sequencing data for *T. podura* are available in the European Nucleotide Archive under the following project PRJEB94285. Male genomic reads have been deposited at SRA under the following project PRJNA1293928. RNAseq reads have been deposited at SRA under the following projects: PRJNA1320679, PRJNA1327219. Code and annotations are available here: https://github.com/DarrenJParker/Timema_DC_MSCI_code and will be archived upon acceptance.

Acknowledgments

This work was supported by the European Research Council Consolidator Grant 864672 ("No Sex No Conflict", T.S.), Swiss FNS grant 31003A_182495 (T.S.), the Genoscope, the Commissariat à l'Énergie Atomique et aux Énergies Alternatives (CEA) and France Génomique (ANR-10-INBS-09–08). We thank the Lausanne Genomic Technologies Facility for PacBio library preparation and sequencing.

References

Anders S, Pyl PT, Huber W (2015). HTSeq--a Python framework to work with high-throughput sequencing data. *Bioinformatics* **31**: 166–169.

Bank S, Bradler S (2022). A second view on the evolution of flight in stick and leaf insects (Phasmatodea). *BMC Ecol Evol* **22**: 62.

Bast J, Parker DJ, Dumas Z, Jalvingh KM, Tran Van P, Jaron KS, *et al.* (2018). Consequences of asexuality in natural populations: insights from stick insects. *Mol Biol Evol* **35**: 1668–1677.

Benjamini Y, Hochberg Y (1995). Controlling the false discovery rate: A practical and powerful approach to multiple testing. *J R Stat Soc Series B Stat Methodol* **57**: 289–300.

Bolger AM, Lohse M, Usadel B (2014). Trimmomatic: a flexible trimmer for Illumina sequence data. *Bioinformatics* **30**: 2114–2120.

Brockdorff N, Turner BM (2015). Dosage compensation in mammals. *Cold Spring Harb Perspect Biol* **7**: a019406.

Brůna T, Hoff KJ, Lomsadze A, Stanke M, Borodovsky M (2021). BRAKER2: automatic eukaryotic genome annotation with GeneMark-EP+ and AUGUSTUS supported by a protein database. *NAR Genom Bioinform* **3**: lqaa108.

Brůna T, Lomsadze A, Borodovsky M (2020). GeneMark-EP+: eukaryotic gene prediction with self-training in the space of genes and proteins. *NAR Genom Bioinform* **2**: lqaa026.

Chauhan P, Swaegers J, Guillen RAS, Svensson EI, Wellenreuther M, Hansson B (2021). Genome assembly, sex-biased gene expression and dosage compensation in the damselfly *Ischnura elegans*. *Genomics* **113**: 1828–1837.

Conrad T, Akhtar A (2012). Dosage compensation in *Drosophila melanogaster*: epigenetic fine-tuning of chromosome-wide transcription. *Nat Rev Genet* **13**: 123–134.

Darolti I, Wright AE, Sandkam BA, Morris J, Bloch NI, Farré M, *et al.* (2019). Extreme heterogeneity in sex chromosome differentiation and dosage compensation in livebearers. *Proc Natl Acad Sci U S A* **116**: 19031–19036.

Davis RJ, Belikoff EJ, Scholl EH, Li F, Scott MJ (2018). No blokes is essential for male viability and X chromosome gene expression in the Australian sheep blowfly. *Curr Biol* **28**: 1987–1992.e3.

Defendini H, Prunier-Leterme N, Robin S, Lameiras S, Baulande S, Simon J-C, *et al.* (2025). The release of sexual conflict after sex loss is associated with evolutionary changes in gene expression. *Proc Biol Sci* **292**: 20242631.

Disteche CM (2012). Dosage compensation of the sex chromosomes. *Annu Rev Genet* **46**: 537–560.

Djordjevic J, Tran Van P, Toubiana W, Labédan M, Dumas Z, Aury J-M, *et al.* (2025). Dynamics of X chromosome hyper-expression and inactivation in male tissues during stick insect development. *PLoS Genet* **21**: e1011615.

Dobin A, Davis CA, Schlesinger F, Drenkow J, Zaleski C, Jha S, *et al.* (2013). STAR: ultrafast universal RNA-seq aligner. *Bioinformatics* **29**: 15–21.

560 Dudchenko O, Batra SS, Omer AD, Nyquist SK, Hoeger M, Durand NC, *et al.* (2017). De
561 novo assembly of the Aedes aegypti genome using Hi-C yields chromosome-length
562 scaffolds. *Science* **356**: 92–95.

563 Dumas Z, Toubiana W, Delattre M, Schwander T (2024). Dynamics of recombination, X
564 inactivation and centromere proteins during stick insect spermatogenesis. *bioRxiv*:
565 2024.09.05.611401.

566 Durand NC, Shamim MS, Machol I, Rao SSP, Huntley MH, Lander ES, *et al.* (2016). Juicer
567 provides a one-click system for analyzing loop-resolution Hi-C experiments. *Cell Syst* **3**:
568 95–98.

569 Emms DM, Kelly S (2019). OrthoFinder: phylogenetic orthology inference for comparative
570 genomics. *Genome Biol* **20**: 238.

571 Flintham E, Savolainen V, Otto SP, Reuter M, Mullon C (2025). The maintenance of genetic
572 polymorphism underlying sexually antagonistic traits. *Evol Lett* **9**: 259–272.

573 Flynn JM, Hubley R, Goubert C, Rosen J, Clark AG, Feschotte C, *et al.* (2020).
574 RepeatModeler2 for automated genomic discovery of transposable element families.
575 *Proc Natl Acad Sci U S A* **117**: 9451–9457.

576 Freitas S, Parker DJ, Labédan M, Dumas Z, Schwander T (2023). Evidence for cryptic sex in
577 parthenogenetic stick insects of the genus Timema. *Proceedings of the Royal Society B:*
578 *Biological Sciences* **290**: 20230404.

579 Gu L, Walters JR (2017). Evolution of sex chromosome dosage compensation in animals: a
580 beautiful theory, undermined by facts and bedeviled by details. *Genome Biol Evol* **9**:
581 2461–2476.

582 Hamada FN, Park PJ, Gordadze PR, Kuroda MI (2005). Global regulation of X chromosomal
583 genes by the MSL complex in Drosophila melanogaster. *Genes Dev* **19**: 2289–2294.

584 Hu Q-L, Ye Y-X, Zhuo J-C, Huang H-J, Li J-M, Zhang C-X (2022). Chromosome-level
585 assembly, dosage compensation and sex-biased gene expression in the small brown
586 planthopper, Laodelphax striatellus. *Genome Biol Evol* **14**: evac160.

587 Jaron KS, Parker DJ, Anselmetti Y, Van PT, Bast J, Dumas Z, *et al.* (2022). Convergent
588 consequences of parthenogenesis on stick insect genomes. *Science Advances* **8**:
589 eabg3842.

590 Kalita AI, Keller Valsecchi CI (2024). Dosage compensation in non-model insects - progress
591 and perspectives. *Trends Genet*.

592 Kalita AI, Marois E, Kozielska M, Weissing FJ, Jaouen E, Möckel MM, *et al.* (2023). The sex-
593 specific factor SOA controls dosage compensation in Anopheles mosquitoes. *Nature*
594 **623**: 175–182.

595 Kelley RL, Solovyeva I, Lyman LM, Richman R, Solovyev V, Kuroda MI (1995). Expression
596 of msl-2 causes assembly of dosage compensation regulators on the X chromosomes
597 and female lethality in Drosophila. *Cell* **81**: 867–877.

598 Kolmogorov M, Yuan J, Lin Y, Pevzner PA (2019). Assembly of long, error-prone reads
599 using repeat graphs. *Nat Biotechnol* **37**: 540–546.

600 Koren S, Walenz BP, Berlin K, Miller JR, Bergman NH, Phillippy AM (2017). Canu: scalable
601 and accurate long-read assembly via adaptive k-mer weighting and repeat separation.

602 *Genome Res* **27**: 722–736.

603 Kriventseva EV, Kuznetsov D, Tegenfeldt F, Manni M, Dias R, Simão FA, *et al.* (2019).
604 OrthoDB v10: sampling the diversity of animal, plant, fungal, protist, bacterial and viral
605 genomes for evolutionary and functional annotations of orthologs. *Nucleic Acids Res* **47**:
606 D807–D811.

607 Krzywinska E, Ribeca P, Ferretti L, Hammond A, Krzywinski J (2023). A novel factor
608 modulating X chromosome dosage compensation in Anopheles. *Curr Biol* **33**: 4697–
609 4703.e4.

610 Laetsch DR, Blaxter ML (2017). BlobTools: Interrogation of genome assemblies. *F1000Res*
611 **6**: 1287.

612 Larose C, Lavanchy G, Freitas S, Parker DJ, Schwander T (2022). Facultative
613 parthenogenesis in an asexual stick insect: re-evolution of sex or vestigial sexual
614 capacity? *bioRxiv*: 2022.03.25.485836.

615 Larsson J, Svensson MJ, Stenberg P, Mäkitalo M (2004). Painting of fourth in genus
616 Drosophila suggests autosome-specific gene regulation. *Proc Natl Acad Sci U S A* **101**:
617 9728–9733.

618 Lee JT (2000). Disruption of imprinted X inactivation by parent-of-origin effects at Tsix. *Cell*
619 **103**: 17–27.

620 Li H (2013). Aligning sequence reads, clone sequences and assembly contigs with BWA-
621 MEM. *arXiv*: 1303.3997.

622 Li H (2018). Minimap2: pairwise alignment for nucleotide sequences. *Bioinformatics* **34**:
623 3094–3100.

624 Li X, Mank JE, Ban L (2024). The grasshopper genome reveals long-term gene content
625 conservation of the X Chromosome and temporal variation in X Chromosome evolution.
626 *Genome Res* **34**: 997–1007.

627 Mahajan S, Bachtrog D (2015). Partial dosage compensation in Strepsiptera, a sister group
628 of beetles. *Genome Biol Evol* **7**: 591–600.

629 Mank JE (2013). Sex chromosome dosage compensation: definitely not for everyone.
630 *Trends Genet* **29**: 677–683.

631 Mank JE, Hosken DJ, Wedell N (2011). Some inconvenient truths about sex chromosome
632 dosage compensation and the potential role of sexual conflict. *Evolution* **65**: 2133–2144.

633 Marin R, Cortez D, Lamanna F, Pradeepa MM, Leushkin E, Julien P, *et al.* (2017).
634 Convergent origination of a Drosophila-like dosage compensation mechanism in a
635 reptile lineage. *Genome Res* **27**: 1974–1987.

636 McKee BD, Handel MA (1993). Sex chromosomes, recombination, and chromatin
637 conformation. *Chromosoma* **102**: 71–80.

638 Metzger DCH, Sandkam BA, Darolti I, Mank JE (2021). Rapid Evolution of Complete Dosage
639 Compensation in Poecilia. *Genome Biol Evol* **13**.

640 Meyer BJ (2000). Sex in the worm: counting and compensating X-chromosome dose.
641 *Trends Genet* **16**: 247–253.

642 Namekawa SH, Lee JT (2009). XY and ZW: is meiotic sex chromosome inactivation the rule
643 in evolution? *PLoS Genet* **5**: e1000493.

644 Nawrocki EP, Eddy SR (2013). Infernal 1.1: 100-fold faster RNA homology searches.
645 *Bioinformatics* **29**: 2933–2935.

646 Page N, Taxiarchi C, Tonge D, Kuburic J, Chesters E, Kriezis A, *et al.* (2023). Single-cell
647 profiling of Anopheles gambiae spermatogenesis defines the onset of meiotic silencing
648 and premeiotic overexpression of the X chromosome. *Commun Biol* **6**: 850.

649 Pal A, Vicoso B (2015). The X Chromosome of Hemipteran insects: conservation, dosage
650 compensation and sex-biased expression. *Genome Biol Evol* **7**: 3259–3268.

651 Parker DJ, Djordjevic J, Schwander T (2019). Olfactory proteins in *Timema* stick insects.
652 *Frontiers in Ecology and Evolution* **7**: 101.

653 Parker DJ, Jaron KS, Dumas Z, Robinson-Rechavi M, Schwander T (2022). X chromosomes
654 show relaxed selection and complete somatic dosage compensation across Timema
655 stick insect species. *J Evol Biol*.

656 Pease JB, Hahn MW (2012). Sex chromosomes evolved from independent ancestral linkage
657 groups in winged insects. *Mol Biol Evol* **29**: 1645–1653.

658 Prince EG, Kirkland D, Demuth JP (2010). Hyperexpression of the X chromosome in both
659 sexes results in extensive female bias of X-linked genes in the flour beetle. *Genome*
660 *Biol Evol* **2**: 336–346.

661 Quinlan AR, Hall IM (2010). BEDTools: a flexible suite of utilities for comparing genomic
662 features. *Bioinformatics* **26**: 841–842.

663 Rayner JG, Hitchcock TJ, Bailey NW (2021). Variable dosage compensation is associated
664 with female consequences of an X-linked, male-beneficial mutation. *Proc Biol Sci* **288**:
665 20210355.

666 Richard G, Legeai F, Prunier-Leterme N, Bretaudeau A, Tagu D, Jaquiéry J, *et al.* (2017).
667 Dosage compensation and sex-specific epigenetic landscape of the X chromosome in
668 the pea aphid. *Epigenetics Chromatin* **10**: 30.

669 Roach MJ, Schmidt SA, Borneman AR (2018). Purge Haplotigs: allelic contig reassignment
670 for third-gen diploid genome assemblies. *BMC Bioinformatics* **19**: 460.

671 Robinson MD, McCarthy DJ, Smyth GK (2010). edgeR: a Bioconductor package for
672 differential expression analysis of digital gene expression data. *Bioinformatics* **26**: 139–
673 140.

674 Rose G, Krzywinska E, Kim J, Revuelta L, Ferretti L, Krzywinski J (2016). Dosage
675 compensation in the African Malaria Mosquito *Anopheles gambiae*. *Genome Biol Evol* **8**:
676 411–425.

677 Schoenmakers S, Wassenaar E, Hoogerbrugge JW, Laven JSE, Grootegoed JA, Baarends
678 WM (2009). Female meiotic sex chromosome inactivation in chicken. *PLoS Genet* **5**:
679 e1000466.

680 Schwander T, Crespi BJ (2009). Multiple direct transitions from sexual reproduction to
681 apomictic parthenogenesis in *Timema* stick insects. *Evolution* **63**: 84–103.

682 Schwander T, Crespi BJ, Gries R, Gries G (2013). Neutral and selection-driven decay of

683 sexual traits in asexual stick insects. *Proc Biol Sci* **280**: 20130823.

684 Schwander T, Henry L, Crespi BJ (2011). Molecular evidence for ancient asexuality in
685 *Timema* stick insects. *Curr Biol* **21**: 1129–1134.

686 Seppey M, Manni M, Zdobnov EM (2019). BUSCO: Assessing genome assembly and
687 annotation completeness. *Methods Mol Biol* **1962**: 227–245.

688 Smith A, Hubley R, Green P (2013). RepeatMasker Open-4.0. *RepeatMasker Open-40*.

689 Stanke M, Keller O, Gunduz I, Hayes A, Waack S, Morgenstern B (2006). AUGUSTUS: ab
690 initio prediction of alternative transcripts. *Nucleic Acids Res* **34**: W435–9.

691 Straub T, Gilfillan GD, Maier VK, Becker PB (2005). The Drosophila MSL complex activates
692 the transcription of target genes. *Genes Dev* **19**: 2284–2288.

693 Toups MA, Vicoso B (2023). The X chromosome of insects likely predates the origin of class
694 Insecta. *Evolution* **77**: 2504–2511.

695 Toups MA, Vicoso B (2025). Insect sex chromosome evolution: conservation, turnover, and
696 mechanisms of dosage compensation. *Curr Opin Insect Sci*: 101411.

697 Vaser R, Sović I, Nagarajan N, Šikić M (2017). Fast and accurate de novo genome
698 assembly from long uncorrected reads. *Genome Res* **27**: 737–746.

699 Vicoso B, Bachtrog D (2015). Numerous transitions of sex chromosomes in Diptera. *PLoS*
700 *Biol* **13**: e1002078.

701 Walker BJ, Abeel T, Shea T, Priest M, Abouelliel A, Sakthikumar S, *et al.* (2014). Pilon: an
702 integrated tool for comprehensive microbial variant detection and genome assembly
703 improvement. *PLoS One* **9**: e112963.

704